JGR Atmospheres

RESEARCH ARTICLE
10.1029/2019JD030559

Fine-Scale Variability of Observed and Simulated Surface Albedo Over the Southern Great Plains

Larry K. Berg[1], Charles N. Long[2], Evgueni I. Kassianov[1], Duli Chand[1], Sheng-Lun Tai[1], Zhao Yang[1], Laura D. Riihimaki[2], Sébastien C. Biraud[3], Jerry Tagestad[1], Alyssa Matthews[1], Albert Mendoza[1], Fan Mei[1], Jason Tomlinson[1], and Jerome D. Fast[1]

[1]Pacific Northwest National Laboratory, Richland, WA, USA, [2]NOAA-CIRES, Boulder, CO, USA, [3]Lawrence Berkeley National Laboratory, Berkeley, CA, USA

Key Points:
- Observed and simulated broadband surface albedo are presented
- Spatial variability of surface albedo is described
- Aircraft and satellite measurements of surface albedo are compared to results from the Weather Research and Forecasting model simulations

Correspondence to:
L. K. Berg,
larry.berg@pnnl.gov

Citation:
Berg, L. K., Long, C. N., Kassianov, E. I., Chand, D., Tai, S.-L., Yang, Z., et al. (2020). Fine-scale variability of observed and simulated surface albedo over the southern Great Plains. *Journal of Geophysical Research: Atmospheres*, *125*, e2019JD030559. https://doi.org/10.1029/2019JD030559

Received 28 FEB 2019
Accepted 11 MAR 2020
Accepted article online 16 MAR 2020

Abstract Surface albedo can be highly variable in both space and time. The Department of Energy's Holistic Interactions of Shallow Clouds, Aerosols, and Land-Ecosystems field study provides a unique opportunity to characterize the variability of surface albedo over the Southern Great Plains of the United States using integrated tower, aircraft, and satellite observations. The primary advantage of the aircraft and satellite observations is the ability to examine the spatial distribution of surface albedo over a large area, while the tower measurements have the ability to examine both diurnal and day-to-day variability at a single location. In general, consistency was found between the broadband (BB) albedo measured from the surface, air, and space. There was a small increase from 0.186 to 0.194 in the aircraft BB surface albedo between May and September (about 4% change), while the Moderate Resolution Imaging Spectroradiometer black-sky BB surface albedo increased from 0.151 to 0.166 over the same period (about 10% change), while the standard deviations in the aircraft and Moderate Resolution Imaging Spectroradiometer BB albedo were similar. The largest seasonal differences in the aircraft BB albedo were found for areas with winter wheat or forest, while areas with pasture or grasses showed a smaller seasonal diversity. The Weather Research and Forecasting model was used to simulate the BB surface albedo. In comparison with the aircraft and satellite observations, the Weather Research and Forecasting-simulated BB surface albedo had no seasonal change and a much narrower distribution.

Plain Language Summary The sunlight reflected by the surface has a large impact on the amount of energy that is available to warm the surface or evaporate water either standing on the surface or trapped in the soil. There are three primary ways to measure the reflection: using tower, aircraft, or satellite. Each approach has advantages and disadvantages, including different fields of view, the wide range of land use under the aircraft and satellite flight tracks, and corrections to account for scattering and absorption of sunlight by clouds and particles in the atmosphere. In this study, we compare tower, aircraft, and satellite measurements made during the Holistic Interactions of Shallow Clouds, Aerosols, and Land-Ecosystems field study. We find differences in the amount of energy that is reflected, which changes with season and we highlight that the differences can be related to land use. We compare observations to simulations completed using the Weather Research and Forecasting model. The modeled reflectance shows little seasonal change and tends to underestimate the variability of the reflectance. These results have significant impacts for other studies focused on the amount of sunlight that is absorbed at the surface and the impact on land-atmosphere interactions.

1. Introduction and Motivation

The surface albedo is a critical component of the surface energy budget that affects how much solar radiation is available to be portioned into the sensible, latent, and soil heat fluxes. Errors in the surface albedo have been shown to contribute to errors in the near-surface temperature in simulations completed with both regional and global models (e.g., Van Weverberg et al., 2018; Winton, 2006). Several approaches have been used to obtain the surface albedo and its variability over different regions and periods of interest. These approaches include tower-based, airborne, and satellite observations. Satellite observations have large spatial coverage and are a useful tool for estimating the surface albedo at regional and global scales (e.g., He et al., 2014; Liang et al., 2010; Pinker, 1985) despite well-known limitations and challenges associated

with atmospheric corrections (e.g., Pinker, 1985; Zhao et al., 2001), narrowband-broadband conversion (Liang et al., 1999), and coarse temporal resolution associated with polar-orbiting satellites.

Instrumentation deployed on towers, such as those supported by the U.S. Department of Energy Atmospheric Radiation Measurement (ARM) User Facility, can provide high-quality surface albedo data. In comparison with satellite data, tower data have two main advantages: atmospheric correction is not required and high-temporal resolution can be obtained. As pointed out by Berg and Lamb (2016), data collected at the ARM Southern Great Plains (SGP) site have long been used to evaluate satellite estimates of surface albedo (Gao et al., 1998; Minnis et al., 1997; Román et al., 2013). An important disadvantage of tower data is their small footprint that cannot be easily extrapolated to the spatially varying landscape. Kassianov et al. (2014) suggested a creative way to increase the footprint effectively using cloud as a mirror, but their method is limited to mostly overcast conditions during which the surface albedo can be different from its clear-sky counterpart. Airborne or spaceborne measurement platforms have larger footprints and also provide the opportunity to sample a much larger range of surface properties.

Relatively small amounts of aerosol loading at the ARM User Facility and near-nadir solar zenith angles reduced the need for atmospheric corrections required for aircraft and satellite data products, which provide surface albedo over a much larger domain than is possible from a tower (e.g., Coddington et al., 2008; Jäkel et al., 2013; Wendisch et al., 2004). This is especially important for regions where there is spatial variability in surface properties. For example, there is a wide variety of land use and land cover (LULC) around the SGP site associated with the cycle of agricultural crops and native land cover. LULC distributions could have important implications for the spatial variability of boundary layer thermodynamic properties that must be adequately captured in regional and global model simulations. For this reason, the characterization of surface heterogeneity and its impact on thermodynamic properties was one motivation of the Department of Energy Holistic Interactions of Shallow Clouds, Aerosols, and Land-Ecosystems (HI-SCALE; Fast et al., 2019) field study.

While many studies have focused on evaluating estimates of snow albedo in the Weather Research and Forecasting (WRF) model (Oaida et al., 2015; Smirnova et al., 2016; Z. Wang & Zeng, 2010), a much smaller number of reports have aimed to develop improved LULC data sets with advanced estimates of surface albedo (Zhang et al., 2012) or to carefully evaluate the surface albedo estimates applied in the WRF model (Meng et al., 2018). Other work has focused on improving Land Surface Models (LSMs) used in Earth System Models. For example, Lawrence and Chase (2007) used National Aeronautics and Space Administration Moderate Resolution Imaging Spectroradiometer (MODIS) observations to refine the plant functional types used in the Community Land Model v3 that could improve estimates of surface albedo. More recently, Ke et al. (2012) evaluated changes in surface albedo associated with high-resolution land surface parameters. Other studies have highlighted bias and errors in surface albedo in Earth System Models, such as those used in the Coupled Model Intercomparison Project Phase 5 models (Levine & Boos, 2017).

In this study, we combine clear-sky surface albedo data collected during the HI-SCALE field study from three different sources: tower, aircraft, and satellite, to quantify the spatial and temporal variability of the surface albedo and we use that data to evaluate the surface albedo simulated by the WRF model. The manuscript is organized as follows. A description of data sources, including tower, airborne, and satellite measurements used in our analysis, is presented in section 2. Section 3 includes the analysis of broadband (BB) surface albedo. These results highlight the sensitivity of the tower-based measurements to changes in the crop directly under the ARM SGP tower, and the relatively good agreement between the aircraft and MODIS-derived black-sky albedo (BSA). Observations are used to evaluate the WRF model output in section 4, and the comparison highlights that the simulated surface albedo has smaller spatial and seasonal variability than is observed.

2. Data Sources

2.1. Tower

The Department of Energy's ARM User Facility maintains tower-based measurements of BB and spectrally resolved surface albedo at a site located in the SGP of North America (McFarlane et al., 2011). A photograph of the tower and the surrounding area taken during HI-SCALE is shown in Figure 1. BB measurements of

Figure 1. View of the ARM tower (center of the image) from the aircraft during HI-SCALE. The medium green area around the tower was alfalfa during the study period. Note that the structure near the base of the tall tower has an area of approximately 30 m^2, and the structures near the road are approximately 80 m from the tower base.

the upwelling (reflected) and downwelling irradiance were made using Eppley precision spectral pyranometers (http://www.eppleylab.com/). ARM quotes an uncertainty of 2% or 10 W/m^2 (whichever is larger) for the upwelling BB measurements and 4% for the downwelling measurements (Andreas et al., 2018). Spectrally resolved measurements are made using skyward-facing multifilter rotating shadowband radiometers and surface facing multifilter radiometers (MFRs) at six narrowband channels (415, 500, 615, 673, 970, and 940 nm). The largest source of uncertainty in the MFR spectral irradiance measurements comes from the calibration uncertainty. Calibration are done by comparison to a National Institute of Standards and Technology standard spectral lamp and are estimated to be around 4% (Campos & Sisterson, 2015). Data from the radiometers are combined into an ARM data product (Gaustad & Riihimaki, 2004) that includes 10-min averages of both BB and spectrally resolved irradiance, albedo, and associated quality control flags. Only the highest-quality data (quality flags equal to 0) are used here. In this study, we focus on data collected from radiometers mounted 25 m above the surface during the spring, summer, and fall of 2016 that corresponds with the HI-SCALE field study. Assuming approximately two thirds of the total energy comes from a cone with radius slightly larger than the measurement height (Kassianov et al., 2014, Equation A5), than the footprint of the tower-based albedo measurements are a circle approximately 25 m in radius, which is dominated by the alfalfa field surrounding the tower and also includes infrastructure near the tower base.

2.2. Satellite

In this study, we utilize the MODIS satellite MCD43A3 Version 6 Albedo product (Z. Wang et al., 2018) that has been applied in a wide range of studies (e.g., Moody et al., 2008; Schaaf et al., 2002; Z. Wang et al., 2014). This albedo product uses the highest-quality pixel-level data by combining data from MODIS Terra (morning pass) and Aqua (afternoon pass) satellites and defines pixels where the combined MODIS albedo has the highest quality on a daily basis. The MODIS Terra and Aqua satellites overpass the equator at 10:30 a.m. and 1:30 p.m. local time every day. The daily albedo data quality is processed using a 16-day algorithm running at 500-m resolution for a given granule (defined as the area sampled over a 5-min window). Here we considered multiple granules to get the best coverage over the domain of interest. The daily albedo

Table 1
Mean and Standard Deviation of Surface Albedo

Date	AOD	Mean MODIS BSA	Std. Dev. MODIS BSA	Mean aircraft BB albedo	Std. Dev. aircraft BB albedo	Mean WRF BB albedo	Std. Dev. WRF BB albedo
13 May 2016	0.101	0.151	0.0094	0.186	0.014	0.168	0.0030
11 September 2016	0.052	0.164	0.0119	0.200	0.0149	0.174	0.0070
17 September 2016	0.110	0.166	0.0128	0.194	0.0268	0.168	0.0054

Note. AOD determined from ARM surface observations at locations near the flight track. Mean and standard deviation of MODIS BSA, aircraft BB surface albedo, and WRF BB surface albedo. Values from MODIS and WRF are subsampled along the aircraft flight track. WRF results are discussed in section 4.

product is derived from an integration of the bidirectional reflectance distribution function model retrieved from all high-quality directional observations available over a 16-day moving window, temporally weighted to the ninth day.

The MODIS albedo data product provides both directional hemispherical reflectance (BSA) and bihemispherical reflectance (white-sky albedo, WSA) at multiple bands. To cover most of the solar spectrum, we use the shortwave band covering wavelengths between 0.3 and 5.0 μm. The WSA is retrieved by integrating the bidirectional reflectance distribution function at all viewing angles and irradiance directions, while the BSA is derived from the directional hemispherical reflectance. We use the MCD43A3 product to obtain the WSA, BSA, and quality assurance flags of surface albedo along with the quality and uncertainty bits. We use the MCD43A2 product to obtain land type and surface albedo uncertainty flags. Based on previous studies using high-quality MCD43 data, the errors in the MODIS-derived albedo are generally less than 5% but can be as large as 10% (e.g., Cescatti et al., 2012; Roman et al., 2013; Z. Wang et al., 2014, 2018). Both the BSA and WSA can be combined to provide the true surface albedo, also called the blue-sky albedo (e.g., He et al., 2012; Román et al., 2010; Wang et al., 2016), with some additional measurements or assumptions. He et al. (2012) estimated the blue-sky albedo using the WSA, BSA, and the diffuse skylight fraction. In our case the diffuse skylight fraction (derived from the ARM multifilter rotating shadowband radiometer data) is less than 0.08 and the aerosol optical depth was 0.11 or less for the case study days (Table 1). Using the spot calculations for the days in May and September, the difference between the blue-sky albedo and BSA is less than 1% so we simply use the BSA in this study. Other studies have highlighted that near midday the BSA is very similar to the blue-sky albedo, so we used only the MODIS BSA with no additional corrections (e.g., Oleson et al., 2003; Román et al., 2010). On two of the three days (13 May and 17 September), the aircraft flight pattern was essentially centered on local noon, while the flight on 11 September was started earlier in the data (centered on 10:00 local time). The exact length of the aircraft flights varied between approximately 3 and 4 hr. These factors associated with the start time and the flight duration make it difficult to apply a time correction to either the satellite or aircraft data for their detailed comparison. Thus, no additional time-of-day correction was applied.

2.3. Aircraft

The HI-SCALE field study was conducted during the 2016 growing season and included two aircraft intensive operations periods (IOPs) utilizing the Department of Energy's Gulfstream-1 (G-1) aircraft, one in the spring (24 April through 21 May) and one in the late summer/early fall (28 August to 24 September). Details of the HI-SCALE field study and the aircraft payload are documented by Fast et al. (2019). This study utilizes BB irradiance data collected using upward- and downward-looking Delta-T SPN1 pyranometers installed on the top and bottom of the fuselage. The SPN1 is designed to measure both total and diffuse incident solar radiation, and the direct radiation is then computed as the difference between the two with an accuracy of 8% or 10 W/m^2 and were calibrated by Delta-T devices. A tilt correction was applied to the BB data following Long et al. (2010). As an extra precaution, instances in which the aircraft tilt was larger than 10° in magnitude have been excluded from the analysis.

In addition to the SPN1's, upward- and downward-looking MFRs (uncertainty estimated to be 4%, as described in section 2.1) were also mounted on the aircraft. A tilt correction was not initially applied to the MFR data, so there is significant dependence of the measured MFR spectral irradiance on the aircraft

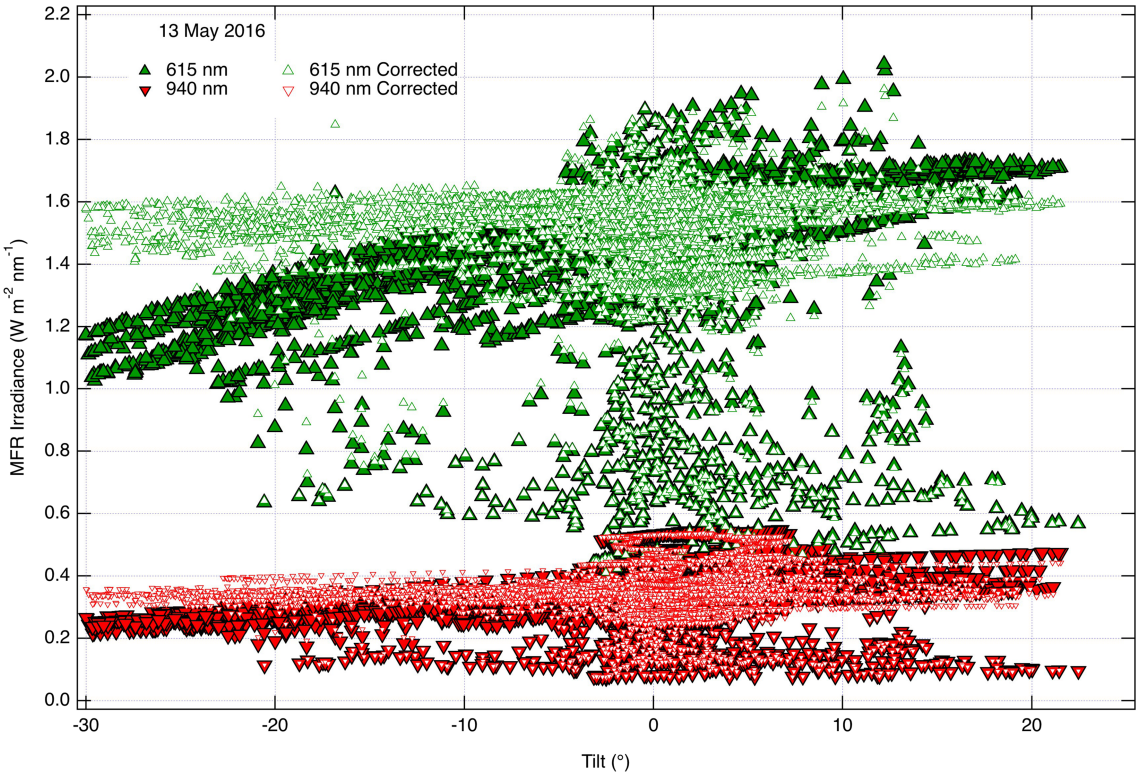

Figure 2. Example of observed (filled) and tilt-corrected (open) upward-looking spectral irradiance at 615 (green upward-pointing triangles) and 940 (red downward-pointing triangles) nm wavelength on 13 May 2016.

tilt (Figure 2). Not surprisingly, there is also a much more pronounced sensitivity to tilt at shorter wavelengths, as shown by the larger slope with tilt for the 615-nm data (filled green symbols in Figure 2) compared to the 940-nm data (red symbols in Figure 2) that can be attributed to differences in the atmospheric scattering at shorter and longer wavelengths. A number of different methods for tilt correction were considered, including application of an empirical fit and deriving a wavelength by wavelength correction based on data such as that shown in Figure 2. This approach, however, would introduce significant uncertainty and it was determined the simplest and best approach was to apply the BB correction of Long et al. (2010) to the MFR data. Overall, applying this correction removes much of the sensitivity to the aircraft tilt, as shown by the open green and red symbols in Figure 2.

Instances in which the direct component of the irradiance is fully or partially blocked by clouds also has a large impact on measurements made with either the SPN1s or the MFRs. For example, the majority of the tilt-corrected 615-nm spectral irradiance data shown in Figure 2 fall between 1.3 and 1.6 $W \cdot m^{-2} \cdot nm^{-1}$. There are instances, however, where the observed tilt corrected spectral irradiance is less than 1.2 $W \cdot m^{-2} \cdot nm^{-1}$, as highlighted by the cluster of points extending to smaller values of irradiance. These periods are likely associated with the presence of clouds above the aircraft and they have a significant impact on the calculation of clear-sky surface albedo. To address this issue, an additional check of the dimensionless ratio of the difference between the direct and diffuse irradiance to the direct irradiance was applied, which is similar to the approach of Long et al. (2006). Time periods where the dimensionless ratio was less than 0.8 (not shown) were assumed to be contaminated by clouds and were excluded from the analysis.

In addition, there were issues with the MFRs for the flights conducted on 15, 17, 20, and 21 September during which the downward-facing MFR reported values that were unrealistically too large. The errors correspond to periods in which the heater controller temperature on the MFR was too large as well. On 17 September, the error first appears at 17:37 UTC and data after that time are excluded from the analysis presented here. The aircraft flight times varied some over the course of the study, with takeoff times on 13 May, 11 September, and 17 September at 11:02, 09:11, and 10:38 Central Standard Time (CST). The

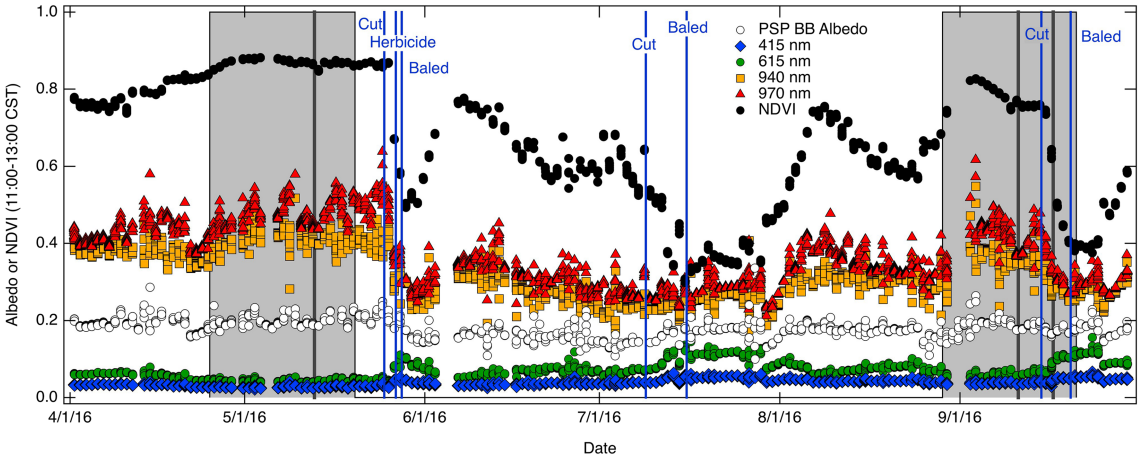

Figure 3. Time series of BB (open circles), 415- (blue), 615- (green), 940- (dark red), and 970-nm (red) surface albedo and normalized difference vegetation index (NDVI; black circles) measured on the ARM tower. Gray boxes indicate aircraft IOPs, and black lines indicate dates of specific HI-SCALE field study flights used in this analysis. Blue lines indicate times when the alfalfa was cut, bailed, or herbicide was applied.

flight duration also varied from day to day so that the flight end times were 14:42, 12:14, and 14:09 CST on 13 May, 11 September, and 17 September.

2.4. LULC

There are several approaches that could be used to identify the LULC under the aircraft. In the context of this study we rely on LULC types derived from a combination of the U.S. Geological Survey National Land Cover and the U.S. Department of Agriculture Cropscape databases (Boryan et al., 2011; Han et al., 2014), which are updated annually with 30-m resolution for the 2016 growing season. Three sets of LULC were derived, based on the type directly below the aircraft and within circles with 200- and 900-m radii, respectively, of the aircraft location at any given time. The LULC data were also spot-checked using downward-looking video on the aircraft.

While the U.S. Geological Survey and U.S. Department of Agriculture LULC data include detailed information about land use and specific crop types, there are fewer details related to forest types. Forests are found throughout the state of Oklahoma, but approximately 45% of the state's forests are located in eastern Oklahoma (Ouachita Mountains, Arkansas Valley, and Ozarks Highlands). This region is the most diverse region of the state and is dominated by a transition zone from oak-pine forests to oak-hickory and post oak-blackjack oak forest types. Species encountered in oak-hickory forest (Ozarks Highlands) include black oak (*Quercus velutina*), white oak (*Quercus alba*), northern red oak (*Quercus rubra*), post oak (*Quercus stellata*), mockernut hickory (*Carya tomentosa*), and bitternut hickory (*Caray cordiformis*). Species encountered in oak-pin (Ouachita Mountain) forests are similar to species encountered in oak-hickory forests but include short leaf pine (*Pinus echinata*). Species encountered in post oak-blackjack forests are post oak (*Q. stellata*) and blackjack oak (*Quercus marilandica*), the two most abundant tree species in Oklahoma.

3. Analysis of Observations

The BB albedo has been derived from the ARM tower measurements for April through October of 2016, which includes both HI-SCALE field study aircraft IOPs. The average midday (observations were taken between 11:00 and 13:00 CST) BB albedo measured by the upward- and downward-looking Eppley precision spectral pyranometeres radiometers on the tower was 0.18 with a standard deviation of 0.02 for the study period (open circles in Figure 3). At first glance, the BB albedo varies little across the spring, summer, and early fall of 2016. Closer examination, however, shows that the BB albedo varies to some extent with the status of the crop under the radiometers, although the fractional change is small. A decrease in BB albedo is found to occur near the end of May and there are increases in BB albedo near the end of July and August. The spectral albedo is very sensitive to the characteristics of the plant canopy within the field of view of the radiometers. The field was planted to alfalfa in the fall of 2015. The first cutting and bailing of the

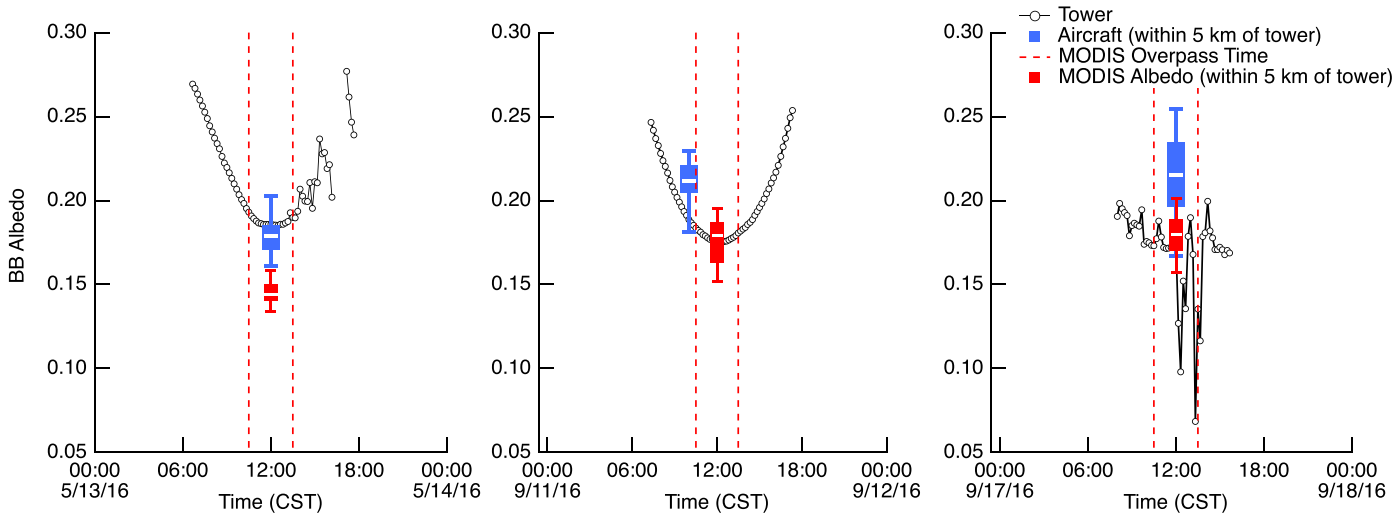

Figure 4. Time series of tower BB surface albedo (open) and box-and-whisker plots of BB surface albedo computed from aircraft (blue) and MODIS (red) measurements. Whiskers indicate 95th and 5th percentiles, while the boxes indicate the 75th and 25th percentiles, and white bars indicate the median for aircraft observations within 5 km of the ARM tower. Red dashed lines represent the approximate MODIS overpass times. Inset pie charts show approximate distribution of crop types under the aircraft flight pattern as described in the text.

alfalfa were conducted from 25 through 26 May, along with the application of herbicide on 27 May. Thus, the marked increase in the surface albedo at 615-nm wavelength and its decrease at both 940- and 970-nm wavelengths right before 1 June 2016 is likely associated with these activities. After 1 June, the alfalfa grows and the 615-nm surface albedo shrinks until the second cutting on 9 July that is also marked by an increase in the 615-nm surface albedo. The field was fertilized on 19 July, and there was a significant increase in albedo until the third cutting on 15 September and subsequent bailing on 20 September. The periods after the cutting are marked by both a decrease in the 940- and 970-nm albedos and an increase in the 615-nm albedo.

One of the flight patterns used during the HI-SCALE field study was designed to map variations of near surface fluxes and albedo in nearly cloud-free conditions. These patterns consisted of a regular north-south or east-west oriented tracks flown relatively close to the surface. Three days, 13 May, 11 September, and 17 September, have been selected for analysis based on the flight pattern and relatively small amounts of cloud cover that were present (0% on 13 May and 11 September and 0–35% on 17 September as derived from the Doppler lidar deployed at the ARM Central Facility; Berg et al., 2017).

The aircraft and satellite observations provide measurements with high spatial resolution. As a first check of the aircraft data and MODIS data, the aircraft and satellite BB surface albedo is compared to BB surface albedo measured by the ARM tower-based measurements. Due to the highly variable nature of LULC and the desire to avoid an atmospheric correction, the comparison is limited to cloud-free cases in which the aircraft was within 5 km of the tower and flying at an altitude below 700 m above ground level or for satellite pixels within 5 km of the tower. Even with these considerations, there is still a significant amount of variability in the aircraft and satellite observations as shown by the box-and-whisker plots in Figure 4. However, there is a reasonably good agreement between the aircraft and tower-based measurements (Figure 4) when these criteria are applied, with the tower observations generally within the range of aircraft observations. The satellite estimates of BB surface albedo (median value of 0.144) are smaller than those obtained from the tower measurements (median value of 0.186) on 13 May. In contrast, the satellite- and tower-based estimates of BB surface albedo observations are comparable for the two days in September. It is also clear from the time series of the tower data that there are significantly more clouds on 17 September than is observed on either of the other study days, making the comparison between the surface albedo obtained from the tower and aircraft measurements more difficult for the portion of the flight track over the tower. Since other portions of the flight track were cloud-free, 17 September was retained in our analysis. The time series of BB surface albedo measured from the tower also highlights the diurnal variability of the BB surface albedo.

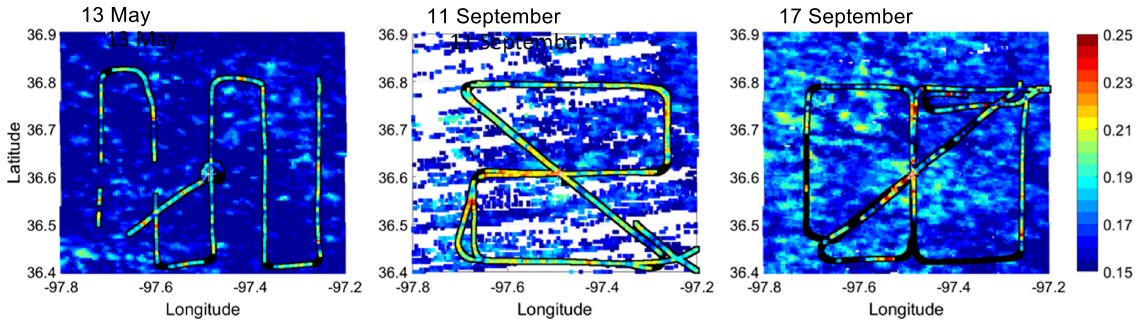

Figure 5. MODIS-derived BSA (background colors) and aircraft derived (tracks) BB surface albedo measured on 13 May, 11 September, and 17 September 2016. Black areas on the flight track indicate missing data. White areas represent either low-quality or missing MODIS data.

The differences in tower measured BB albedo between the MODIS overpass times at 10:30 and 13:30 CST are approximately 4% from 10:30 and 12:00 and approximately 2% from 12:00 and 13:30.

The range of aircraft measured values is likely due, at least in part, to the diversity of crops and land use near the Central Facility. Using the land databases described in section 2.4, the LULC can be derived for the area under the aircraft. Both the BB and spectrally resolved radiation measurements on the aircraft have a hemispheric field of view. Following the discussion of the radiometer footprint presented in section 2.1 and assuming approximately two thirds of the total energy comes from a cone with a radius slightly larger than the measurement height, we can assume that the LULC derived from a circle with 900-m radius provides a reasonable basis for determining the relevant LULC, given that the altitude of the aircraft was less than 700 m above ground level. The most common land use type under the flight track near the Central Facility was winter wheat, but there were also significant amounts of pasture/grass, soybeans, and fallow ground (Figure 4).

The BB surface albedo measured by the radiometers on the aircraft ranges from approximately 0.15 to 0.25 during both IOPs (Figure 5), which is consistent with the BB surface albedo derived from the ARM tower, but is generally larger than the computed MODIS BSA (Table 1). The MODIS BSA albedo computed along the aircraft flight track (Table 1) increases slightly from 0.151 to 0.166 between 13 May and 17 September, a change of approximately 10%, which is larger than the expected uncertainty of approximately 5% of the MODIS measurements. Similar behavior is found for the BB albedo measured from the aircraft, which also increases slightly from 0.186 to 0.194 over the HI-SCALE study period. It is important to note that the aircraft measured BB surface albedo is greatest on 11 September, but this could be associated with the earlier flight time on that day. There are also many more missing MODIS data points on 11 September, although there is still reasonable coverage along the aircraft flight track. Given that this less than a week between 11 and 17 September, only a small difference is expected in the mean surface albedo, which is indeed the case (difference less than 2%). The spatial variability of both the MODIS BSA and aircraft BB albedo increases in the fall compared to the conditions on 13 May as represented by the standard deviations presented in Table 1. The spatial variability of the aircraft BB surface albedo is found to be greater than either the MODIS BSA or the WRF BB surface albedo.

Differences in the MODIS and aircraft measured derived BB surface albedos are highlighted by their distributions (Figures 4 and 6 and Table 1). It is also important to note that the effective spatial resolution of the MODIS data is less than 1 km (Campagnolo et al., 2016), while the effective spatial resolution of the aircraft BB (based on the reasoning described in section 2.1 for the tower-based measurements) ranges between approximately 500 m and 1 km depending on the aircraft altitude. On 13 May, both the mode value and spread of the distribution computed using the aircraft measurements are larger than those seen for the MODIS BSA (Figure 6). The differences in the modes are smaller on 11 September, and the aircraft data are skewed toward smaller values of albedo than on 13 May and 17 September, which could be associated with the early flight time. The MODIS and aircraft distributions are closest on 17 September, but the aircraft values are still generally larger than the MODIS BSA. The underestimation of BB albedo presented here is consistent with results from other studies comparing MODIS BB albedo to tower observations

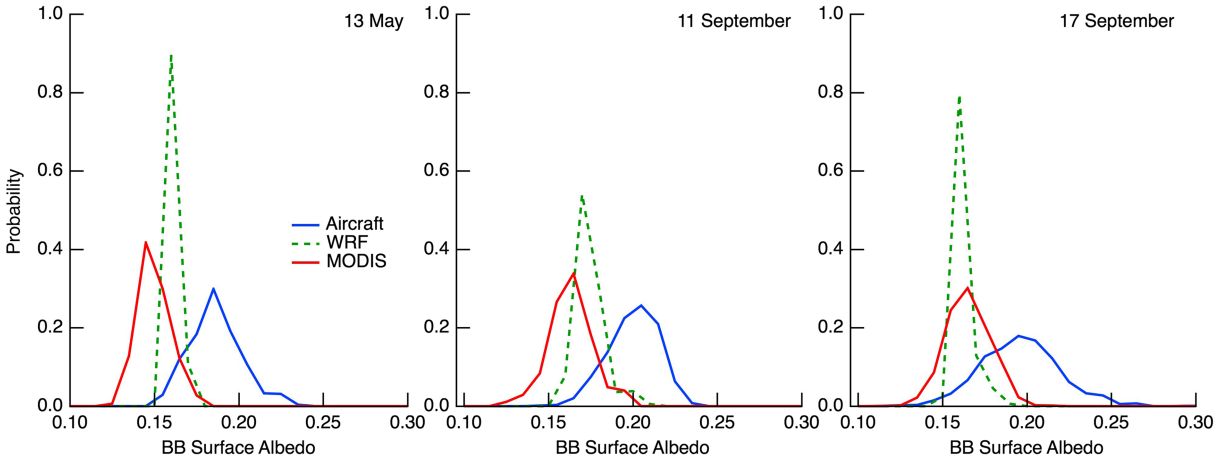

Figure 6. Probability density functions (PDFs) of BB surface albedo from MODIS BSA (red), aircraft (blue) BB albedo, and WRF BB albedo (green) on 13 May, 11 September, and 17 September 2016. WRF results are discussed in section 4.

(Cescatti et al., 2012; Coddington et al., 2008), but others have shown an overestimation (Franch et al., 2013; Knobelspiesse et al., 2008). There are a number of possible explanations for the differences in the MODIS and aircraft data, including differences in pixel size, differences in time of day, surface heterogeneity, ignoring MODIS WSA, differences associated with the time averaging of the MODIS data, and errors associated with the atmospheric correction. In this study, an atmospheric correction factor is not applied to the MODIS BSA data to account for scattering and absorption by aerosol and gases in the atmospheric column. As stated earlier, one advantage of the aircraft derived data analyzed here is the relatively small amount of the atmospheric column between the surface and the aircraft that minimizes the need for any such correction. Finally, as highlighted in Figure 4, there is a significant variation in the albedo over the course of the day, with the smallest values near local solar noon.

In addition to examining the distribution of albedo derived from an entire flight leg, we can also examine the BB albedo obtained when the aircraft was flying over areas in which the LULC were dominated by an individual type. The data were sorted to find cases in which at least 66% of the LULC in the circle with 900-m radius centered on the aircraft location is a single type. While there are many different LULC types in the vicinity of the ARM site, there are three dominant types based on our definition, so we limit the analysis to cases with pasture/grass, winter wheat, and forest.

We find statistically significant differences in the BB albedo associated with LULC between the spring and fall (Figure 7). The BB surface albedo of the pasture/grass does not change much with season, while there are large changes in the BB surface albedo of the winter wheat and forest. During the September flights, the BB surface albedo of the pasture/grass was found to be 0.190 and 0.185, which is approximately the same as the spring value of 0.193. In contrast, the albedo of the winter wheat is much larger in the fall (0.193 and 0.216) than was found in the spring (0.175). The BB surface albedo associated with forest is found to decrease in September compared to May (noting that there are many fewer observations over forest than the pasture or winter wheat as shown in Figure 7). These differences in BB surface albedo are likely due to changes in the plant canopy with season. The differences in the two days in September could be due to differences in the flight tracks (Figure 5) and differences in time of day that can lead to systematic changes in albedo. One important caveat of the results presented in Figure 7 is the differences in the relative sample sizes associated with the flight pattern used on each day. It is important to note that some of the differences seen in this study could be associated with differences in the aircraft flight pattern. In addition, even if the same flight pattern was used, small changes in the aircraft position could lead to analysis of different surface areas.

4. WRF Model Configuration

In this study, observations of BB surface albedo derived from tower, aircraft, and BSA derived from MODIS are compared to output from the WRF model (Skamarock et al., 2008). Within the WRF model, the surface

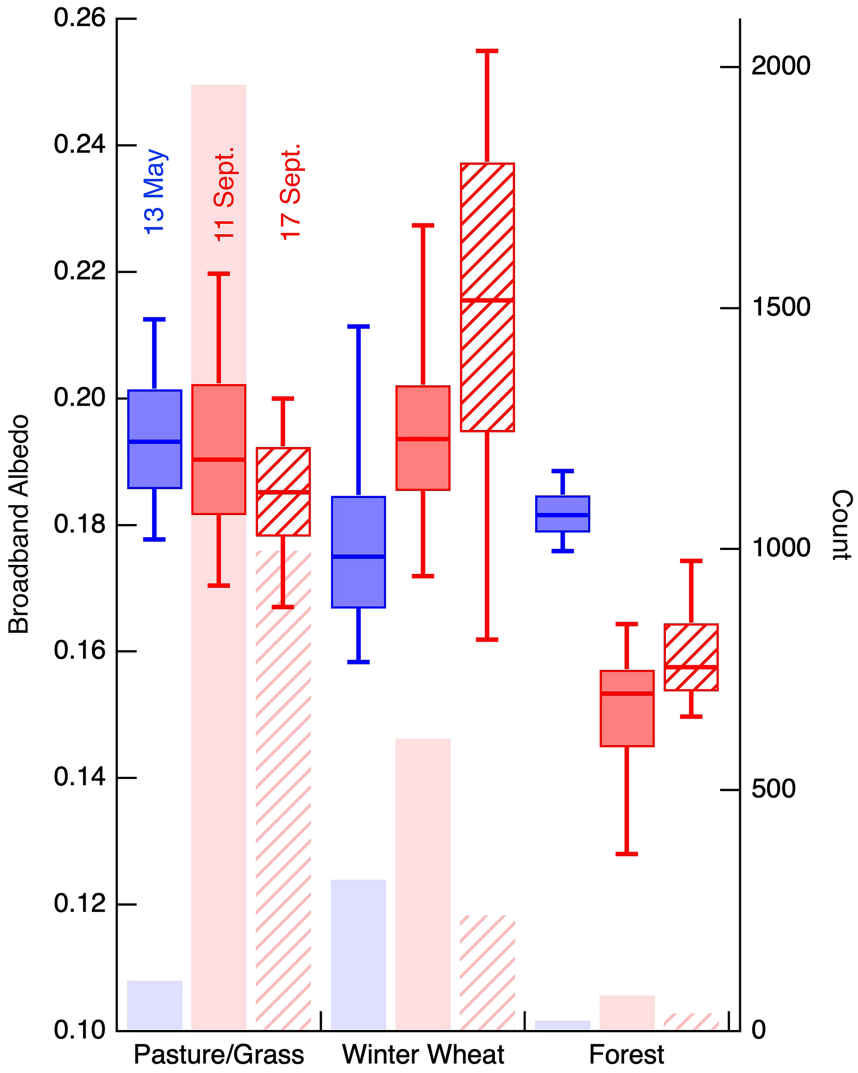

Figure 7. Distributions of aircraft measured BB surface albedo (based on the dominant LULC under the aircraft for 13 May (blue), 11 September (red), and 17 September (hashed). Light shading or symbols indicates the number of observations for each LULC type.

albedo is defined using calculations in the LSM and the details are dependent on the specific LSM that is selected. Here, we utilize the Noah-MP LSM (Niu et al., 2011; Yang et al., 2011). In this LSM the ground albedo is first computed as a function of the soil color and soil moisture in the first model layer. The vegetation effect on the albedo is considered using a modified two-stream method (Dickinson, 1983; Sellers, 1985) that considers the leaf area index (LAI), stem area index (SAI), and green vegetation fraction. In the configuration used in this study the LAI and SAI are specified from the standard input tables provided with WRF and the green vegetation fraction is assumed to be the annual maximum value. Such a configuration is typically applied in many different applications. Other model configurations are possible, including those that use a MODIS climatology to define the LAI, SAI, and green vegetation fraction. The simulated BB albedo is computed directly from the upwelling and downwelling clear-sky fluxes so that no cloud screening is required in the analysis of the model output. Other studies (e.g., Arsenault et al., 2018; Cuntz et al., 2016) have examined the sensitivity of the LSM in the context of the surface energy fluxes.

The WRF model was configured to use four nested domains approximately centered on the ARM SGP Central Facility. The innermost domain used a grid spacing of 1.3 km and 74 vertical levels. The

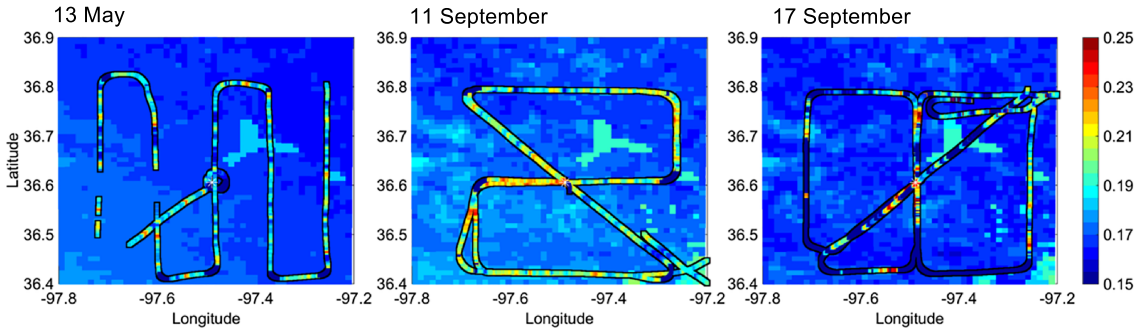

Figure 8. WRF model (background colors) and aircraft derived (tracks) BB surface albedo measured on 13 May, 11 September, and 17 September 2016.

simulations used the RRTMG shortwave and longwave radiation (Iacono et al., 2008). The Morrison two-moment parameterization (Morrison et al., 2009) was used for cloud microphysics. Turbulence was represented using the Mellor-Yamada-Janic parameterization (Mellor & Yamada, 1982). The cumulus parameterization was turned off on the inner-most domain, but the modified Kain-Fritsch cumulus potential (Berg et al., 2013; Kain, 2004; Kain & Fritsch, 1990) parameterization was used on the three outer domains. Each run was started at 00 UTC and run for 36 hr.

5. Simulated BB Albedo

The data sets described in the previous sections provide a unique opportunity to evaluate the BB surface albedo from the WRF model using a typical model configuration. In this simple setup, the LAI, SAI, and green vegetation fraction are extrapolated to a specific date using tables of monthly values provided with the model. While both the MODIS and aircraft data increase by approximately 10% and 4%, respectively (focusing on the conditions observed on 13 May and 17 September due to more consistent flight times), the BB surface albedo from the WRF model does not change significantly between the spring and summer IOPs as shown in Figure 8 and Table 1, although it is generally between the MODIS and aircraft values. Based on analysis of the aircraft data presented in section 3 (Figure 7), the change in observed albedo is dominated by changes associated with the winter wheat and to a lesser extent forest (due to the relatively small amount of forest in the study domain). These results suggest that the values of LAI and SAI in the standard WRF input do not accurately capture the lifecycle of specific crops, such as winter wheat, and may adversely affect simulations of the surface radiation budget around the SGP.

There are also significant differences in the variability of the observed and simulated BB surface albedo. Compared to the observed distributions, the simulated distributions of the BB surface albedo are much narrower and are dominated by a large peak near a value of 0.16, with much smaller peaks at slightly smaller and larger values of BB albedo (Figure 6). As described in section 4, the calculation of albedo in the Noah-MP LSM considers the ground albedo and the vegetation effect separately. The ground albedo is defined using the soil color (which is constant over the domain used in this study), and the soil moisture in the first model level. In the configuration of the WRF model that have used in this study, the LAI, SAI, and green vegetation fraction vary with month as function of the specific land use are used as input to the modified two-stream method that is used to determine impact of the plant canopy on the albedo. Over our study region, the land cover types in the model are dominated by cropland or grassland, which leads to little variability in the simulated BB albedo. Thus, it is the spatial variability of the soil moisture that has the largest impact on the variability of the simulated surface albedo. A fact highlighted by the small values of albedo just northeast of the ARM Central Facility (located at the center of the domain) where the soil type is different than the surrounding area, leading to much smaller soil moisture values and hence larger values of BB surface albedo (Figure 8).

A second set of simulations were completed using LAI, SAI, and green vegetation fraction derived from a multiyear climatology of MODIS observations, but there was not a large impact on the variability of the surface albedo (not shown). These findings argue for the use of revised values of surface albedo derived from relatively high resolution (in both space and time) MODIS or aircraft data that are relevant for a specific

period of time, such as those used in this analysis, that can more accurately represent the time evolution of the lifecycle of the various crop and land use types. This is particularly critical in areas like the SGP where the specific crops in a given field change from year to year or where there is significant year-to-year variability in the in the lifecycle of various crops, such as the timing of the wheat harvest.

The relative differences in the BB surface albedo presented may not be large in an absolute sense, but they have relatively large impact on the amount of energy available at the surface to be partitioned in to the sensible, latent, and soil heat fluxes. For example, near noon on 13 May, the downwelling shortwave radiance is approximately 700 W/m^2 at the SGP site. Given the variability in the WRF BB surface albedo, this leads to a range of available energy at the surface between 585 and 570 W/m^2. For the observed aircraft albedo, the amount of energy ranges between 592 and 534 W/m^2, and for the MODIS-derived albedo the amount of energy ranges between 620 and 564 W/m^2. While beyond the scope of this study, future investigations should evaluate the impact of ignoring the variability on the subsequent boundary layer development.

6. Summary and Conclusions

The BB surface albedo has been computed using three different instrument platforms: a tower-based system at the ARM SGP site, a research aircraft, and MODIS. Each approach has advantages and disadvantages, yet estimates of the BB surface albedo are generally consistent across the platforms. The tower-based measurements show very little change in the BB surface albedo with season, while the aircraft and MODIS measurements indicate a seasonal increase of the BB surface albedo by approximately 4% and 10%, respectively. The measurements of BB surface albedo also show a large amount of spatial variability across the study domain with noticeable increases during the fall that are primarily associated with dry-land wheat and to a lesser extent forests in the study region.

The aircraft and satellite data are compared to the BB surface albedo derived from the WRF model. The WRF model simulations using the Noah-MP LSM is found to underestimate the seasonal change in the BB surface albedo over the study domain. This is likely associated with prescribed values of LAI and SAI that do not accurately describe the life cycle of the crops in the region of the study. The simulated standard deviation of the BB surface albedo is much smaller and dominated by a single peak compared to the smooth and relatively broad distribution provided by either the aircraft or satellite observations. Given the small range of LULC and associated values of LAI, SAI, and green vegetation fraction associated with values that are only a function of the vegetation type, the majority of the spatial variability in the BB surface albedo is associated with variations of soil moisture in the first model layer.

The work presented here highlights the often-underappreciated role of the BB surface albedo in regional-scale simulations and points to shortcomings in a commonly used WRF model configuration. Future studies should focus on the use of high-quality data set, like those described here, to better capture the actual spatial and temporal variability in the BB surface albedo for studies focused on specific dates and times. Additional studies are also needed to investigate how applying climatological values of canopy properties, which were also shown to underestimate the variability and impact the details of land-atmosphere interactions in long-term simulations.

Acknowledgments
The HI-SCALE field study was supported by the Atmospheric Radiation Measurement (ARM) Climate Research Facility and the Environmental Molecular Science Laboratory (EMSL), both are U.S. Department of Energy (DOE) Office of Science User Facilities sponsored by the Office of Biological and Environmental Research. This research was supported by the Atmospheric Science Research (ASR) program as part of the DOE Office of Biological and Environmental Research. MODIS data are provided by NASA EOSDIS Land Processes Distributed Active Archive Center (LP DAAC). Computational resources were provided by Pacific Northwest National Laboratory (PNNL) Institutional Computing. Aircraft and tower data used in this manuscript are available from the ARM Data Archive (https://www.archive.arm.gov/). PNNL is operated by DOE by the Battelle Memorial Institute under Contract DE-A06-76RLO 1830.

References

Andreas, A., Dooraghi, M., Habte, A., Kutchenreiter, M., Reda, I., & Sengupta, M. (2018). Solar infrared radiation station (SIRS), sky radiation (SKYRAD), ground radiation (GNDRAD), and broadband radiometer station (BRS) instrument handbook Rep., Pacific Northwest National Laboratory.

Arsenault, K. R., Nearing, G. S., Wang, S., Yatheendradas, S., & Peters-Lidard, C. D. (2018). Parameter sensitivity of the Noah-MP land surface model with dynamic vegetation. *Journal of Hydrometeorology*, *19*(5), 815–830. https://doi.org/10.1175/jhm-d-17-0205.1

Berg, L. K., Gustafson, W. I., Kassianov, E. I., & Deng, L. (2013). Evaluation of a modified scheme for shallow convection: Implementation of CuP and case studies. *Monthly Weather Review*, *141*(1), 134–147. https://doi.org/10.1175/mwr-d-12-00136.1

Berg, L. K., & Lamb, P. J. (2016). Surface properties and interactions: Coupling the land and atmosphere within the ARM program. *Meteorological Monographs*, *57*, 23.21–23.17. https://doi.org/10.1175/amsmonographs-d-15-0044.1

Berg, L. K., Newsom, R. K., & Turner, D. D. (2017). Year-long vertical velocity statistics derived from Doppler lidar data for the continental convective boundary layer. *Journal of Applied Meteorology and Climatology*, *56*(9), 2441–2454. https://doi.org/10.1175/jamc-d-16-0359.1

Boryan, C., Yang, Z., Mueller, R., & Craig, M. (2011). Monitoring US agriculture: The US Department of Agriculture, National Agricultural Statistics Service, cropland data layer program AU—Boryan, Claire. *Geocarto International*, *26*(5), 341–358. https://doi.org/10.1080/10106049.2011.562309

Campagnolo, M. L., Sun, Q., Liu, Y., Schaaf, C., Wang, Z., & Román, M. O. (2016). Estimating the effective spatial resolution of the operational BRDF, albedo, and nadir reflectance products from MODIS and VIIRS. *Remote Sensing of Environment*, *175*, 52–64. https://doi.org/10.1016/j.rse.2015.12.033

Campos, E., & Sisterson D. (2015). A unified approach for reporting ARM measurement uncertainties technical Report. Rep DOE/SC-ARM-TR-170, DOE ARM Climate Resesarch Facility, Washington DC.

Cescatti, A., Marcolla, B., Santhana Vannan, S. K., Pan, J. Y., Román, M. O., Yang, X., et al. (2012). Intercomparison of MODIS albedo retrievals and in situ measurements across the global FLUXNET network. *Remote Sensing of Environment*, *121*, 323–334. https://doi.org/10.1016/j.rse.2012.02.019

Coddington, O., Schmidt, K. S., Pilewskie, P., Gore, W. J., Bergstrom, R. W., Román, M., et al. (2008). Aircraft measurements of spectral surface albedo and its consistency with ground-based and space-borne observations. *Journal of Geophysical Research*, *113*, D17209. https://doi.org/10.1029/2008JD010089

Cuntz, M., Mai, J., Samaniego, L., Clark, M., Wulfmeyer, V., Branch, O., et al. (2016). The impact of standard and hard-coded parameters on the hydrologic fluxes in the Noah-MP land surface model. *Journal of Geophysical Research: Atmospheres*, *121*, 10,676–610,700. https://doi.org/10.1002/2016jd025097

Dickinson, R. E. (1983). Land surface processes and climate—Surface albedos and energy balance. In B. Saltzman (Ed.), *Advances in geophysics* (pp. 305–353). New York: Elsevier. https://doi.org/10.1016/S0065-2687(08)60176-4

Fast, J. D., Berg, L. K., Alexander, L., Bell, D., D'Ambro, E., Hubbe, J., et al. (2019). Overview of the HI-SCALE field campaign: A new perspective on shallow convective clouds. *Bulletin of the American Meteorological Society*, *100*(5), 821–840. https://doi.org/10.1175/bams-d-18-0030.1

Franch, B., Oltra-Carrió, R., Vermote, E. F., & Fedele, E. (2013). Evaluation of the MODIS albedo product over a heterogeneous agricultural area AU-Sobrino. *International Journal of Remote Sensing*, *34*(15), 5530–5540. https://doi.org/10.1080/01431161.2013.792968

Gao, W., Coulter, R. L., Lesht, B. M., Qiu, J., & Wesely, M. L. (1998). Estimating clear-sky regional surface fluxes in the Southern Great Plains Atmospheric Radiation Measurement site with ground measurements and satellite observations. *Journal of Applied Meteorology*, *37*(1), 5–22. https://doi.org/10.1175/1520-0450(1998)037<0005:ecsrsf>2.0.co;2

Gaustad, K. L., & Riihimaki L. D. (2004). Surface spectral albedo (SURFSPECALB1MLAWER), edited by a. R. M. A. C. R. Facility. https://doi.org/10.5439/1095394

Han, W., Yang, Z., Di, L., & Yue, P. (2014). A geospatial web service approach for creating on-demand cropland data layer thematic maps. *Transactions of the ASABE*, *57*(1), 239–247. https://doi.org/10.13031/trans.57.10020

He, T., Liang, S., & Song, D. X. (2014). Analysis of global land surface albedo climatology and spatial-temporal variation during 1981–2010 from multiple satellite products. *Journal of Geophysical Research: Atmospheres*, *119*, 10,281–10,298. https://doi.org/10.1002/2014JD021667

He, T., Liang, S., Wang, D., Wu, H., Yu, Y., & Wang, J. (2012). Estimation of surface albedo and directional reflectance from Moderate Resolution Imaging Spectroradiometer (MODIS) observations. *Remote Sensing of Environment*, *119*, 286–300. https://doi.org/10.1016/j.rse.2012.01.004

Iacono, M. J., Delamere, J. S., Mlawer, E. J., Shephard, M. W., Clough, S. A., & Collins, W. D. (2008). Radiative forcing by long-lived greenhouse gases: Calculations with the AER radiative transfer models. *Journal of Geophysical Research*, *113*, D13103. https://doi.org/10.1029/2008jd009944

Jäkel, E., Wendisch, M., & Mayer, B. (2013). Influence of spatial heterogeneity of local surface albedo on the area-averaged surface albedo retrieved from airborne irradiance measurements. *Atmospheric Measurement Techniques*, *6*(3), 527–537. https://doi.org/10.5194/amt-6-527-2013

Kain, J. S. (2004). The Kain–Fritsch convective parameterization: An update. *Journal of Applied Meteorology*, *43*(1), 170–181. https://doi.org/10.1175/1520-0450(2004)043<0170:tkcpau>2.0.co;2

Kain, J. S., & Fritsch, J. M. (1990). A one-dimensional entraining/detraining plume model and its application in convective parameterization. *Journal of the Atmospheric Sciences*, *47*(23), 2784–2802. https://doi.org/10.1175/1520-0469(1990)047<2784:aodepm>2.0.co;2

Kassianov, E., Barnard, J., Flynn, C., Riihimaki, L., Michalsky, J., & Hodges, G. (2014). Areal-averaged spectral surface albedo from ground-based transmission data alone: Toward an operational retrieval. *Atmosphere*, *5*(3), 597.

Ke, Y., Leung, L. R., Huang, M., Coleman, A. M., Li, H., & Wigmosta, M. S. (2012). Development of high resolution land surface parameters for the Community Land Model. *Geoscientific Model Development*, *5*(6), 1341–1362. https://doi.org/10.5194/gmd-5-1341-2012

Knobelspiesse, K. D., Cairns, B., Schmid, B., Román, M. O., & Schaaf, C. B. (2008). Surface BRDF estimation from an aircraft compared to MODIS and ground estimates at the Southern Great Plains site. *Journal of Geophysical Research*, *113*, D20105. https://doi.org/10.1029/2008JD010062

Lawrence, P. J., & Chase, T. N. (2007). Representing a new MODIS consistent land surface in the Community Land Model (CLM 3.0). *Journal of Geophysical Research*, *112*, G01023. https://doi.org/10.1029/2006JG000168

Levine, X. J., & Boos, W. R. (2017). Land surface albedo bias in climate models and its association with tropical rainfall. *Geophysical Research Letters*, *44*, 6363–6372. https://doi.org/10.1002/2017GL072510

Liang, S., Strahler, A. H., & Walthall, C. (1999). Retrieval of land surface albedo from satellite observations: A simulation study. *Journal of Applied Meteorology*, *38*(6), 712–725. https://doi.org/10.1175/1520-0450(1999)038<0712:rolsaf>2.0.co;2

Liang, S., Wang, K., Zhang, X. F., & Wild, M. (2010). Review on estimation of land surface radiation and energy budgets from ground measurement, remote sensing and model simulations. *IEEE Journal of Selected Topics in Applied Earth Observations and Remote Sensing*, *3*(3), 225–240. https://doi.org/10.1109/JSTARS.2010.2048556

Long, C. N., Ackerman, T. P., Gaustad, K. L., & Cole, J. N. S. (2006). Estimation of fractional sky cover from broadband shortwave radiometer measurements. *Journal of Geophysical Research*, *111*, D11204. https://doi.org/10.1029/2005jd006475

Long, C. N., Bucholtz, A., Jonsson, H. H., Schmid, B., Vogelmann, A. M., & Wood, J. (2010). A method of correcting for tilt from horizontal in downwelling shortwave irradiance measurements on moving platforms. *The Open Atmospheric Science Journal*, *4*, 78–87. https://doi.org/10.2174/1874282301004010078

McFarlane, S. A., Gaustad, K. L., Mlawer, E. J., Long, C. N., & Delamere, J. (2011). Development of a high spectral resolution surface albedo product for the ARM Southern Great Plains central facility. *Atmospheric Measurement Techniques*, *4*(9), 1713–1733. https://doi.org/10.5194/amt-4-1713-2011

Mellor, G. L., & Yamada, T. (1982). Development of a turbulence closure-model for geophysical fluid problems. *Reviews of Geophysics*, *20*(4), 851–875. https://doi.org/10.1029/RG020i004p00851

Meng, X., Lyu, S., Zhang, T., Zhao, L., Li, Z., Han, B., et al. (2018). Simulated cold bias being improved by using MODIS time-varying albedo in the Tibetan Plateau in WRF model. *Environmental Research Letters*, *13*(4), 044028. https://doi.org/10.1088/1748-9326/aab44a

Minnis, P., Mayor, S., Smith, W. L., & Young, D. F. (1997). Asymmetry in the diurnal variation of surface albedo. *IEEE Transactions on Geoscience and Remote Sensing*, *35*(4), 879–890. https://doi.org/10.1109/36.602530

Moody, E. G., King, M. D., Schaaf, C. B., & Platnick, S. (2008). MODIS-derived spatially complete surface albedo products: Spatial and temporal pixel distribution and zonal averages. *Journal of Applied Meteorology and Climatology*, *47*(11), 2879–2894. https://doi.org/10.1175/2008jamc1795.1

Morrison, H., Thompson, G., & Tatarskii, V. (2009). Impact of cloud microphysics on the development of trailing stratiform precipitation in a simulated squall line: Comparison of one- and two-moment schemes. *Monthly Weather Review*, *137*(3), 991–1007. https://doi.org/10.1175/2008mwr2556.1

Niu, G.-Y., et al. (2011). The community Noah land surface model with multiparameterization options (Noah-MP): 1. Model description and evaluation with local-scale measurements. *Journal of Geophysical Research*, *116*, D12109. https://doi.org/10.1029/2010JD015139

Oaida, C. M., Xue, Y., Flanner, M. G., Skiles, S. M., Sales, F. D., & Painter, T. H. (2015). Improving snow albedo processes in WRF/SSiB regional climate model to assess impact of dust and black carbon in snow on surface energy balance and hydrology over western U. S. *Journal of Geophysical Research: Atmospheres*, *120*, 3228–3248. https://doi.org/10.1002/2014JD022444

Oleson, K. W., Bonan, G. B., Schaaf, C., Gao, F., Jin, Y., & Strahler, A. (2003). Assessment of global climate model land surface albedo using MODIS data. *Geophysical Research Letters*, *30*(8), 1443. https://doi.org/10.1029/2002GL016749

Pinker, R. T. (1985). Determination of surface albedo from satellites. *Advances in Space Research*, *5*(6), 333–343. https://doi.org/10.1016/0273-1177(85)90338-2

Román, M. O., Gatebe, C. K., Shuai, Y., Wang, Z., Gao, F., Masek, J., et al. (2013). Use of in situ and airborne multiangle data to assess MODIS- and Landsat-based estimates of directional reflectance and albedo. *IEEE Transactions on Geoscience and Remote Sensing*, *51*(3). https://doi.org/10.1109/TGRS.2013.2243457

Roman, M. O., Gatebe, C. K., Shuai, Y., Wang, Z., Gao, F., Masek, J. G., et al. (2013). Use of in situ and airborne multiangle data to assess MODIS- and Landsat-based estimates of directional reflectance and albedo. *IEEE Transactions on Geoscience and Remote Sensing*, *51*(3), 1393–1404. https://doi.org/10.1109/TGRS.2013.2243457

Román, M. O., Schaaf, C. B., Lewis, P., Gao, F., Anderson, G. P., Privette, J. L., et al. (2010). Assessing the coupling between surface albedo derived from MODIS and the fraction of diffuse skylight over spatially-characterized landscapes. *Remote Sensing of Environment*, *114*(4), 738–760. https://doi.org/10.1016/j.rse.2009.11.014

Schaaf, C. B., Gao, F., Strahler, A. H., Lucht, W., Li, X., Tsang, T., et al. (2002). First operational BRDF, albedo nadir reflectance products from MODIS. *Remote Sensing of Environment*, *83*(1-2), 135–148. https://doi.org/10.1016/S0034-4257(02)00091-3

Sellers, P. J. (1985). Canopy reflectance, photosynthesis and transpiration. *International Journal of Remote Sensing*, *6*(8), 1335–1372. https://doi.org/10.1080/01431168508948283

Skamarock, W. C., Klemp, M. B., Dudhia, J., Gill, D. O., Barker, D. M., Duda, M. G., et al. (2008). A description of the advanced research WRF version 3Rep. NCAR/TN-475+STR, NCAR.

Smirnova, T. G., Brown, J. M., Benjamin, S. G., & Kenyon, J. S. (2016). Modifications to the rapid update cycle land surface model (RUC LSM) available in the Weather Research and Forecasting (WRF) model. *Monthly Weather Review*, *144*(5), 1851–1865. https://doi.org/10.1175/mwr-d-15-0198.1

van Weverberg, K., Morcrette, C. J., Petch, J., Klein, S. A., Ma, H. Y., Zhang, C., et al. (2018). CAUSES: Attribution of surface radiation biases in NWP and climate models near the U.S. Southern Great Plains. *Journal of Geophysical Research: Atmospheres*, *123*, 3612–3644. https://doi.org/10.1002/2017JD027188

Wang, D., Zhu, B., Jiang, Z., Yang, X.-Q., & Zhu, T. (2016). The impact of the direct effects of sulfate and black carbon aerosols on the subseasonal march of the East Asian subtropical summer monsoon. *Journal of Geophysical Research: Atmospheres*, *121*, 2610–2625. https://doi.org/10.1002/2015JD024574

Wang, Z., Schaaf, C. B., Strahler, A. H., Chopping, M. J., Román, M. O., Shuai, Y., et al. (2014). Evaluation of MODIS albedo product (MCD43A) over grassland, agriculture and forest surface types during dormant and snow-covered periods. *Remote Sensing of Environment*, *140*, 60–77. https://doi.org/10.1016/j.rse.2013.08.025

Wang, Z., Schaaf, C. B., Sun, Q., Shuai, Y., & Román, M. O. (2018). Capturing rapid land surface dynamics with collection V006 MODIS BRDF/NBAR/albedo (MCD43) products. *Remote Sensing of Environment*, *207*, 50–64. https://doi.org/10.1016/j.rse.2018.02.001

Wang, Z., & Zeng, X. (2010). Evaluation of snow albedo in land models for weather and climate studies. *Journal of Applied Meteorology and Climatology*, *49*(3), 363–380. https://doi.org/10.1175/2009jamc2134.1

Wendisch, M., Pilewskie, P., Jäkel, E., Schmidt, S., Pommier, J., Howard, S., et al. (2004). Airborne measurements of areal spectral surface albedo over different sea and land surfaces. *Journal of Geophysical Research*, *109*, D08203. https://doi.org/10.1029/2003JD004392

Winton, M. (2006). Surface albedo feedback estimates for the AR4 climate models. *Journal of Climate*, *19*(3), 359–365. https://doi.org/10.1175/jcli3624.1

Yang, Z.-L., Niu, G. Y., Mitchell, K. E., Chen, F., Ek, M. B., Barlage, M., et al. (2011). The community Noah land surface model with multiparameterization options (Noah-MP): 2. Evaluation over global river basins. *Journal of Geophysical Research*, *116*, D12110. https://doi.org/10.1029/2010JD015140

Zhang, C., Wang, Y., Lauer, A., & Hamilton, K. (2012). Configuration and evaluation of the WRF model for the study of Hawaiian regional climate. *Monthly Weather Review*, *140*(10), 3259–3277. https://doi.org/10.1175/mwr-d-11-00260.1

Zhao, W., Tamura, M., & Takahashi, H. (2001). Atmospheric and spectral corrections for estimating surface albedo from satellite data using 6S code. *Remote Sensing of Environment*, *76*(2), 202–212. https://doi.org/10.1016/S0034-4257(00)00204-2